



## OPEN ACCESS

## EDITED BY

Mohammad Shoab,  
Shaqra University, Saudi Arabia

## REVIEWED BY

Rizwan Ahmad,  
Aligarh Muslim University, India  
Salisu Dan'Azumi,  
Bayero University Kano, Nigeria

## \*CORRESPONDENCE

Zhanyong Feng,  
✉ 1731676204@qq.com

RECEIVED 17 April 2024

ACCEPTED 03 June 2024

PUBLISHED 16 July 2024

## CITATION

Zhou J, Feng Z, Li Y, Wang J, Meng X, Liu Y  
and Qiu S (2024), Identification of dominant  
tree species based on Resource-1 02D  
hyperspectral image data.  
*Front. Earth Sci.* 12:1418865.  
doi: 10.3389/feart.2024.1418865

## COPYRIGHT

© 2024 Zhou, Feng, Li, Wang, Meng, Liu and  
Qiu. This is an open-access article distributed  
under the terms of the [Creative Commons  
Attribution License \(CC BY\)](https://creativecommons.org/licenses/by/4.0/). The use,  
distribution or reproduction in other forums is  
permitted, provided the original author(s) and  
the copyright owner(s) are credited and that  
the original publication in this journal is cited,  
in accordance with accepted academic  
practice. No use, distribution or reproduction  
is permitted which does not comply with  
these terms.

# Identification of dominant tree species based on Resource-1 02D hyperspectral image data

Jingchun Zhou<sup>1,2,3</sup>, Zhanyong Feng<sup>1,2,3\*</sup>, Yiping Li<sup>1,2,3</sup>,  
Jinliang Wang<sup>1</sup>, Xiangrui Meng<sup>1,2,3</sup>, Yuan Liu<sup>1,2,3</sup> and  
Shaobo Qiu<sup>1,2,3</sup>

<sup>1</sup>Faculty of Geography, Yunnan Normal University, Kunming, China, <sup>2</sup>Yunnan Key Laboratory of Resources and Environmental Remote Sensing for Universities in Yunnan, Kunming, China, <sup>3</sup>Center for Geospatial Information Engineering and Technology of Yunnan Province, Kunming, China

Fine-grained classification of tree species by using high-spectral image data has garnered considerable attention from scholars. In this study, through field measurements from Maguan County, Wenshan Prefecture, Yunnan Province, China, high-spectral image data from the Chinese Resource-1 02D satellite were used as the data source. Various analyses were conducted on the original image's spectral curve, the spectral curve after envelope removal, the spectral curve after first-order differential transformation, and the spectral curve after second-order differential transformation. A spectral angle mapping classification method was employed to classify and identify four dominant tree species in Maguan County, and the accuracy of the classification results was validated using a confusion matrix. Results indicate that the highest accuracy in tree species classification was achieved when first-order differential transformation and envelope removal were used for the spectral curve; the overall accuracy exceeded 95%, and the kappa value was approximately 0.95. The classification results for the spectral curve after second-order differential transformation were the lowest, with an overall accuracy of 81.69% and a kappa value of 0.76. This research demonstrates that applying first-order differential transformation or envelope removal in combination with spectral angle mapping classification considerably reduces data processing time and improves tree species classification accuracy.

## KEYWORDS

hyperspectral imaging, tree species identification, spectral curve, spectral angle classification, confusion matrix

## 1 Introduction

Forest ecosystems are essential components of the earth's ecosystems. They provide suitable living spaces for flora and fauna while playing a crucial role in environmental protection (Evans, 1939), climate (Herawati and Santoso, 2011) regulation (Thompson et al., 2009), soil and water conservation (Molchanov, 1963), windbreak and sand fixation (Rong et al., 2022), and ecological improvement (Sayer et al., 2004) In recent years, ecological issues (Sovacool, 2014; Liu et al., 2018), such as greenhouse gas emissions, soil erosion, soil degradation, loss of biodiversity, and decreasing water resources, have become increasingly prominent because of forest degradation. Therefore, conducting forest resource

inventory to comprehensively and accurately assess the quantity and quality of forest resources has become an indispensable task for governments, forestry departments, and forest management units. This task supports ecological conservation, sustainable forestry development, and modern forest management.

Traditional methods of forest inventory primarily rely on manual surveys, which are characterized by high labor intensity; substantial workload; low efficiency; and high time, labor, and financial costs. Moreover, the complexity of the geographical environment poses risks to survey personnel. As a result, the use of remote sensing technology for forest resource inventory has gradually become a research focus for domestic and international scholars (Leckie, 1990; Boyd and Danson, 2005). Remote sensing images have also become a vital data source in forest resource identification and monitoring (Lei et al., 2016; Pasquarella et al., 2018).

Identifying the types, distribution, and quantity of trees is a crucial aspect of forest resource inventory, and the use of remote sensing imagery for tree species classification has elicited widespread attention from scholars. In early studies, multispectral imagery was an important data source in tree species classification (Zhong et al., 2021). However, its spectral resolution is limited, so accurately differentiating tree species with a similar spectral reflectance is difficult. Typically, only two broad categories, namely, coniferous and broadleaf forests, can be distinguished (Yu, 2013). Hyperspectral imagery presents a new opportunity for fine-grained tree species classification (Zhang et al., 2018), and the use of valuable information within hyperspectral data for precise tree species classification has become a popular research direction (Wang, 2011). Scholars have conducted various studies in this area. For example, Gong et al. used artificial neural networks and successfully classified one broadleaf and six coniferous tree species with an accuracy of up to 90% (Gong et al., 1998). Martin M E et al. combined hyperspectral data to classify 11 tree species on the basis of spectral characteristics and leaf features (Martin et al., 1998). Kumar et al. used 11 sets of leaf spectral reflectance data to differentiate tree species and demonstrated the enhanced distinctiveness of the spectral feature curves after first-order differential transformation (Kumar et al., 2010). In addition, Goodenough et al. classified five forest tree species in Victoria, Canada, by using hyperspectral data and obtained high accuracy of up to 92.9% (Goodenough et al., 2002). Gong Peng et al. used data obtained from a spectrometer to identify six tree species types (Gong et al., 1997). Ding Lixia et al. utilized an envelope removal method and Euclidean distance to identify four tree species and achieved promising results (Ding et al., 2010). Moreover, Wang Lu et al. used HJ-2A hyperspectral imagery to recognize dominant tree species in the Tahe region of Greater Khingan Mountains and achieved the highest accuracy in tree species classification after applying second-order differential transformation to the imagery (Wang and Fan, 2015). Despite these advancements, challenges remain in tree species classification. Machine-based classification methods often require high-quality imagery and are time consuming, leading to reduced classification accuracy. Meanwhile, spectral feature-based methods can be influenced by the spectral signatures of other land cover types, resulting in low classification accuracy and quality. This study combined differential transformation and spectral angle classification

methods to enhance the accuracy and general applicability of tree species classification.

This study, which was based on forest inventory field measurements in Maguan County, Wenshan Zhuang and Miao Autonomous Prefecture, Yunnan Province, China, and used high-spectral-resolution remote sensing imagery from the Resource-1 02D satellite, focused on four dominant tree species in Maguan County (*Pinus yunnanensis*, Alder, *Quercus*, and China fir). It employed a combination of differential transformation and spectral angle classification methods to develop an efficient, accurate approach for dimensionality reduction and fine-grained classification of tree species by using high-spectral-resolution remote sensing imagery. The study's findings offer a new, effective method of utilizing spaceborne high-spectral-resolution remote sensing imagery data in forest resource classification and inventory work. This method provides a novel approach and solution and offers reliable data support for forest resource conservation and scientific management.

## 2 Research area and data

### 2.1 Study area

Maguan County is located in the southwestern part of Wenshan Zhuang and Miao Autonomous Prefecture, Yunnan Province, China. Its geographical coordinates range from approximately 22°42' to 23°15' north latitude and 103°52' to 104°39' east longitude. It is situated in the southeastern part of Yunnan Province on a low-latitude plateau and is characterized by typical karst topography, as depicted in Figure 1. Maguan County has a diverse and complex terrain, with elevations ranging from a minimum of 123 m to a maximum of 2,579 m above sea level. Consequently, the vertical variation in climate is much more pronounced than the horizontal variation. The region experiences an annual average temperature of 16.9°C, with July being the hottest month (average of 21.7°C) and January being the coldest (average of 9.7°C). The area receives an annual average rainfall of 1,345 mm, enjoys an average of 1,804 h of annual sunlight, and has a frost-free period averaging 327 days, indicating that the area has a subtropical eastern monsoon climate. Maguan County is rich in forestry resources and has high biodiversity, and its forest coverage rate is 56.7%. The county encompasses a total forested area of 163,160 ha, with a total live wood volume of 7.95 million m<sup>3</sup>. It is primarily home to subtropical evergreen broadleaf forests, mixed coniferous and broadleaf forests, and plantations of tung oil, tea oil, tea, and lacquer trees. This study focused on four dominant tree species in Maguan County, namely, *P. yunnanensis*, Alder, *Quercus*, and China fir.

### 2.2 Data

The fundamental data used in this study are outlined in Table 1. The data primarily include the following.

- (1) Resource-1 02D Hyperspectral Image Data: These data have three images in total, that is, two from 10 November 2020, and

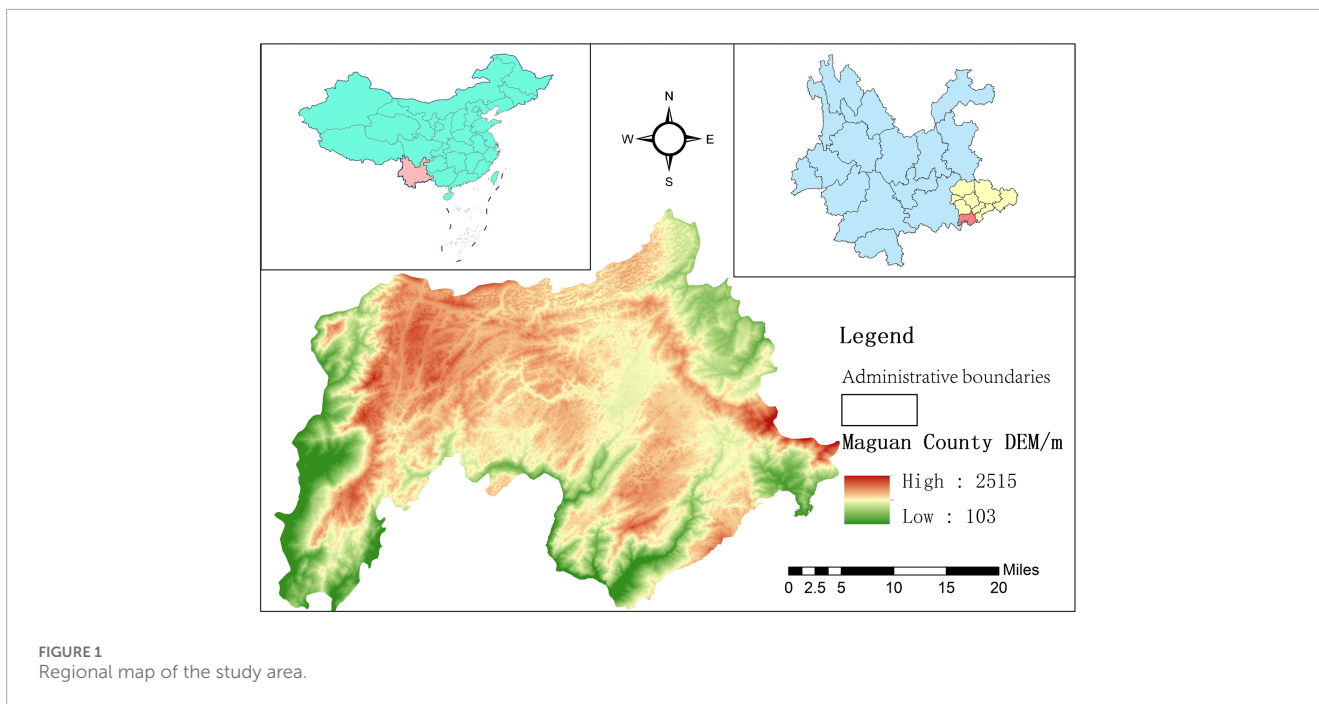


**TABLE 1** Basic data of the study area.

Data name	Data sources	Main purpose
Resource 1 02D hyperspectral image data	<a href="https://data.cresda.cn/#/home">https://data.cresda.cn/#/home</a>	Used for tree species classification
Administrative boundary of Maguan County	<a href="http://datav.aliyun.com/portal/school/atlas/area_selector">http://datav.aliyun.com/portal/school/atlas/area_selector</a>	Produce regional administrative boundary maps
DEM elevation	NASA EARTHDATA	Produce a topographic thematic map of Maguan County
Landsat8 OLI imaging	<a href="https://www.gscloud.cn/search">https://www.gscloud.cn/search</a>	Geometric correction of hyperspectral data by using thematic maps of the terrain in Maguan County
Lin Ban's field investigations	Forestry Bureau of Maguan County	Spectral characteristic curves for collecting major tree species

one from 6 March 2021, and cover the entire Maguan County region.

- (2) Maguan County Administrative Boundary Data: These data provide information on the administrative boundaries of Maguan County.
- (3) Digital Elevation Model (DEM) Data: These data offer elevation information on the study area.
- (4) Landsat 8 Operational Land Imager (OLI) Data: These data are utilized for various analyses.
- (5) Forest Stand Data from Field Surveys: These are obtained from the Maguan County Forestry Bureau and include a total of 8,510 forest stands for the four tree species. Specifically, the data contain 618 *P. yunnanensis* stands, 1,546 China fir stands, 4,135 Alder stands, and 2,211 Quercus stands.

### 3 Research methods

The overall technical approach used in this study is depicted in Figure 2, and the primary research methods are described in the following subsections.

#### 3.1 Data preprocessing

Hyperspectral data are characterized by numerous spectral bands; they contain a wealth of information and often have high data redundancy. Therefore, hyperspectral data need to be preprocessed. The main steps involve the removal of redundant bands, radiometric correction, atmospheric correction, and geometric correction.

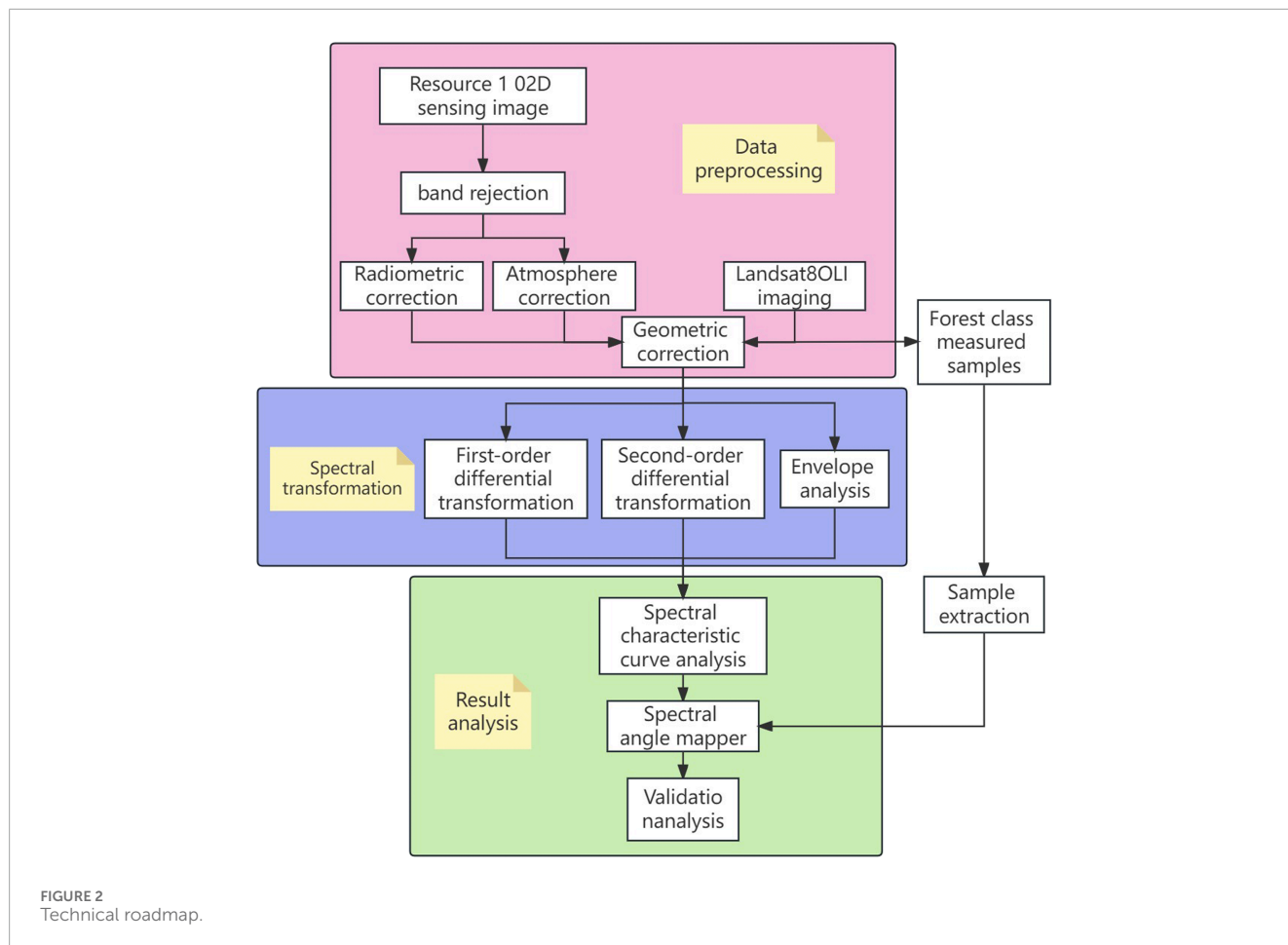


FIGURE 2 Technical roadmap.

TABLE 2 Excluded bands of Resource-1 02D satellite.

Bands	Reason	Range/nm
VN: 72–76	Fusion bands	1,005–1,040
SW: 22–27	Water vapor-affected bands	1,357–1,442
SW: 48–59		1,795–1,980
SW: 82–83		2,366–2,384
SW: 88–90	Low signal-to-noise ratio bands	2,467–2,501

The preprocessing procedure in this study began by loading the hyperspectral image via Envi software. Then, the spectral characteristic curves of each band were exported from the image. Subsequently, in Excel, specific bands were removed from the Resource-1 02D hyperspectral image. These excluded bands included fusion bands, water vapor-affected bands, and bands with low signal-to-noise ratios (Table 2). Only the necessary bands for the study were retained, and these included visible and near-infrared (VN) bands 1–71 (395–996 nm), shortwave infrared (SW) bands 1–21 (1,005–1,341 nm), bands 28–47 (1,459–1,778 nm), bands 60–81 (1,997–2,350 nm), and bands 84–87 (2,400–2,450 nm).

Next, the Resource-1 02D hyperspectral image was subjected to radiometric calibration and atmospheric correction by using the FLAASH atmospheric correction tool in ENVI software. This process eliminated atmospheric aerosols and other substances that could affect image quality, allowing the image to reflect the true surface reflectance. Figure 3 shows the vegetation spectral reflectance curve before atmospheric correction, and Figure 4 displays the vegetation spectral reflectance curve after atmospheric correction. Afterward, the Resource-1 02D hyperspectral image was geometrically corrected using Landsat 8 OLI imagery as a reference to ensure that the image’s errors were less than 0.5 pixels.

### 3.2 Spectral transformation

Applying differential transformation to hyperspectral data can effectively enhance image quality, reduce the influence of the background on vegetation spectral information, improve the signal-to-noise ratio, and further eliminate the effects of atmospheric interference during transformation. Differential transformation allows for a highly accurate representation of the biological composition information of different vegetation types (Shu et al., 2016). This study focused on three transformation methods: first-order differential transformation, second-order differential transformation, and envelope removal.

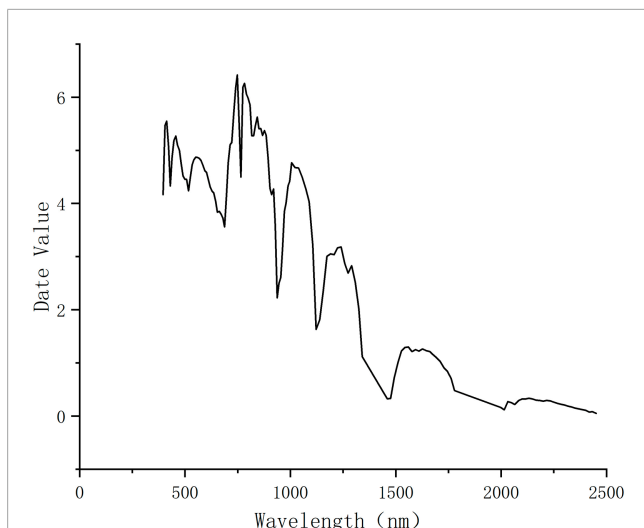


FIGURE 3  
Spectral reflectance curve of vegetation before calibration.

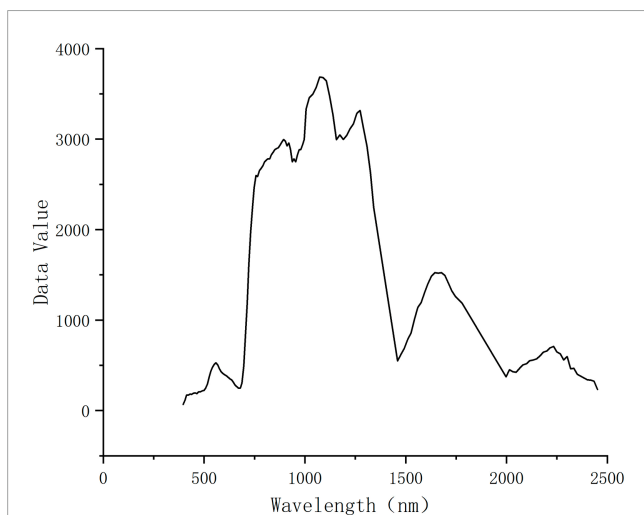


FIGURE 4  
Corrected vegetation spectral reflectance curve.

### 3.2.1 Spectral first-order differential transformation

Spectral first-order differential transformation involves taking the first derivative of the original remote sensing image data (Gu et al., 2019; Shen, 2022). After this transformation, the image data are less affected by atmospheric radiation, scattering, and atmospheric absorption, enabling the spectral curves to reveal subtle differences between land cover types (Sun et al., 2019). The calculation for spectral first-order differential transformation is given as Eq. 1

$$FDR_{\lambda t} = \frac{dR}{d\lambda} = \frac{R_{\lambda t+1} - R_{\lambda t}}{\Delta\lambda} \quad (1)$$

where  $\lambda t$  represents the wavelength of the  $t$ -th spectral band;  $FDR_{\lambda t}$  is the spectral first-order differential value between the  $t$ -th and  $t+1$ -th spectral bands;  $R_{\lambda t}$  and  $R_{\lambda t+1}$  are the original spectral reflectance

values for the  $t$ -th and  $t+1$ -th spectral bands, respectively; and  $\Delta\lambda$  is generally set to 1.

### 3.2.2 Spectral second-order differential transformation

Second-order differential transformation involves taking the second derivative of the original remote sensing image data (Yang et al., 2021; Ma et al., 2023). After this transformation, the image data can further amplify differences between different land cover types, thus aiding in identifying sensitive spectral bands (Liu, 2021). The calculation for spectral second-order differential transformation is given as Eq. 2

$$SDR_{\lambda t} = \frac{d^2R}{d\lambda^2} = \frac{d}{d\lambda} \left( \frac{dR}{d\lambda} \right) = \frac{R_{\lambda t+2} + 2R_{\lambda t+1} + R_{\lambda t}}{(\Delta\lambda)^2} \quad (2)$$

where  $\lambda t$  represents the wavelength of the  $t$ -th spectral band;  $FDR_{\lambda t}$  is the spectral second-order differential value between the  $t$ -th and  $t+2$ -th spectral bands;  $R_{\lambda t}$  and  $R_{\lambda t+1}$  and  $R_{\lambda t+2}$  are the original spectral reflectance values for the  $t$ -th,  $t+1$ -th, and  $t+2$ -th spectral bands, respectively; and  $\Delta\lambda$  is generally set to 1.

### 3.2.3 Envelope line division method

The envelope removal method, also known as the continuum subtraction method (Kokaly and Clark, 1999; Ren et al., 2020), is effective in enhancing the absorption, reflection, and emission characteristics of spectral curves. It normalizes the spectral curves to a consistent spectral background, facilitating the comparison of characteristic values between different spectral curves. The reflectance values after envelope removal are normalized to a range between 0 and 1 (Roush and Clark, 1984), with the peak point being one and the other points being less than 1. The final result is the continuum-removed data (Meng et al., 2020). The calculation for envelope removal is presented as Eq. 3

$$R_{Ck} = \frac{R_k}{R_{crk}} \quad (3)$$

where  $R_{Ck}$  represents the continuum-removed value for the  $k$ -th spectral band,  $R_k$  is the original spectral reflectance for the  $k$ -th spectral band, and  $R_{Crk}$  represents the continuum for the  $k$ -th spectral band (Xie et al., 2005).

## 3.3 Spectral angle mapping method

Spectral angle mapping (SAM) (Xu et al., 2013; Yu et al., 2016) was introduced by Kruse et al., in 1993 (Kruse et al., 1993). The principle behind using this method in land cover classification is to treat the spectral signature of each pixel in an image as a high-dimensional vector. It measures the spectral similarity between two vectors by calculating the angle between them. A small angle indicates high spectral similarity and a high likelihood that the pixels belong to the same land cover class (Petropoulos et al., 2013; Zhang and Li, 2014). Therefore, unknown data can be categorized based on the size of the spectral angle. In this study, for tree species classification, the spectral angle between unknown and known data was computed, and the unknown data were assigned to the

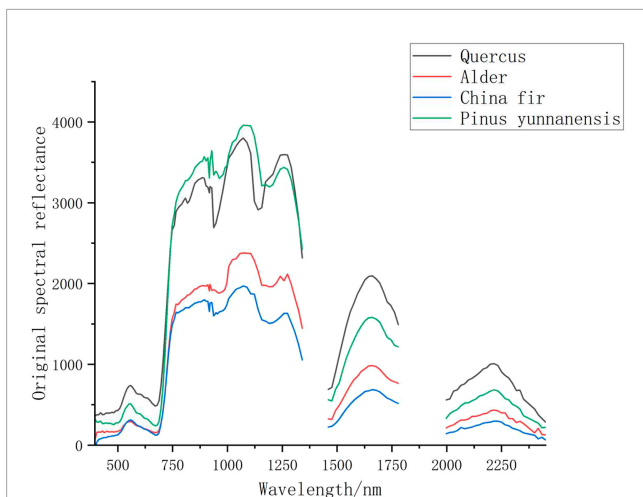


FIGURE 5 Original spectral characteristic curves of the four vegetation types.

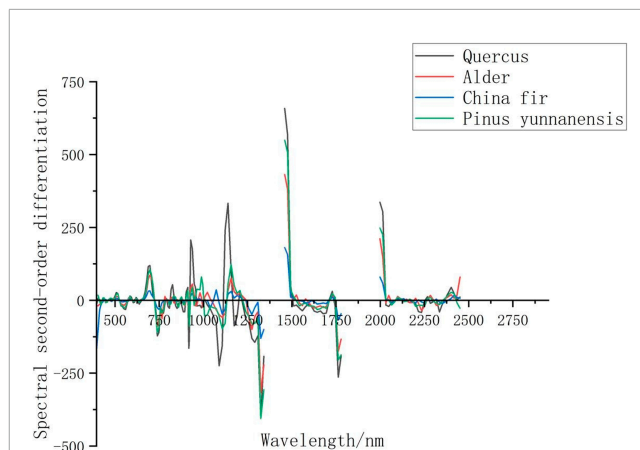


FIGURE 7 Vegetation curve obtained through second-order differential transformation.

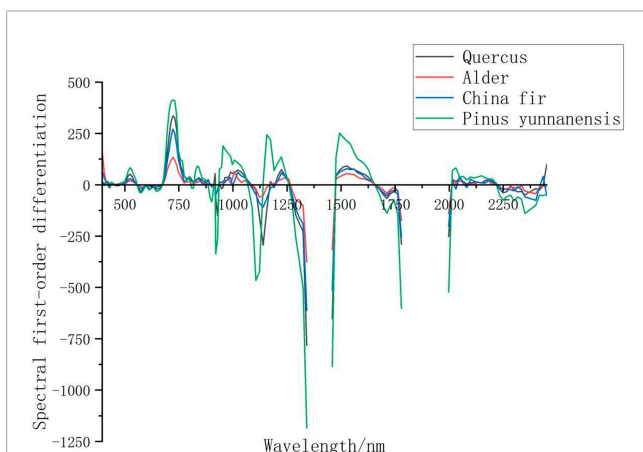


FIGURE 6 Vegetation curve obtained through first-order differential transformation.

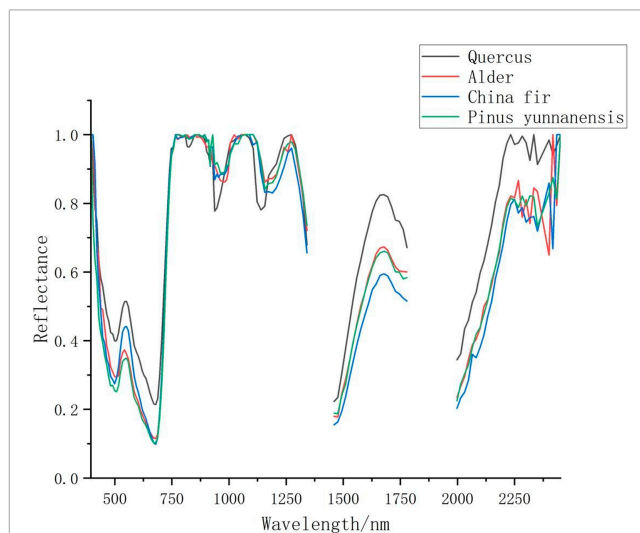


FIGURE 8 Vegetation curve after envelope removal.

class corresponding to the smallest spectral angle. The calculation formula for SAM is Eq. 4

$$\cos \alpha = \frac{\sum_{i=1}^n (x_i \cdot y_i)}{\left( \sqrt{\sum_{i=1}^n x_i^2} \cdot \sqrt{\sum_{i=1}^n y_i^2} \right)} \quad (4)$$

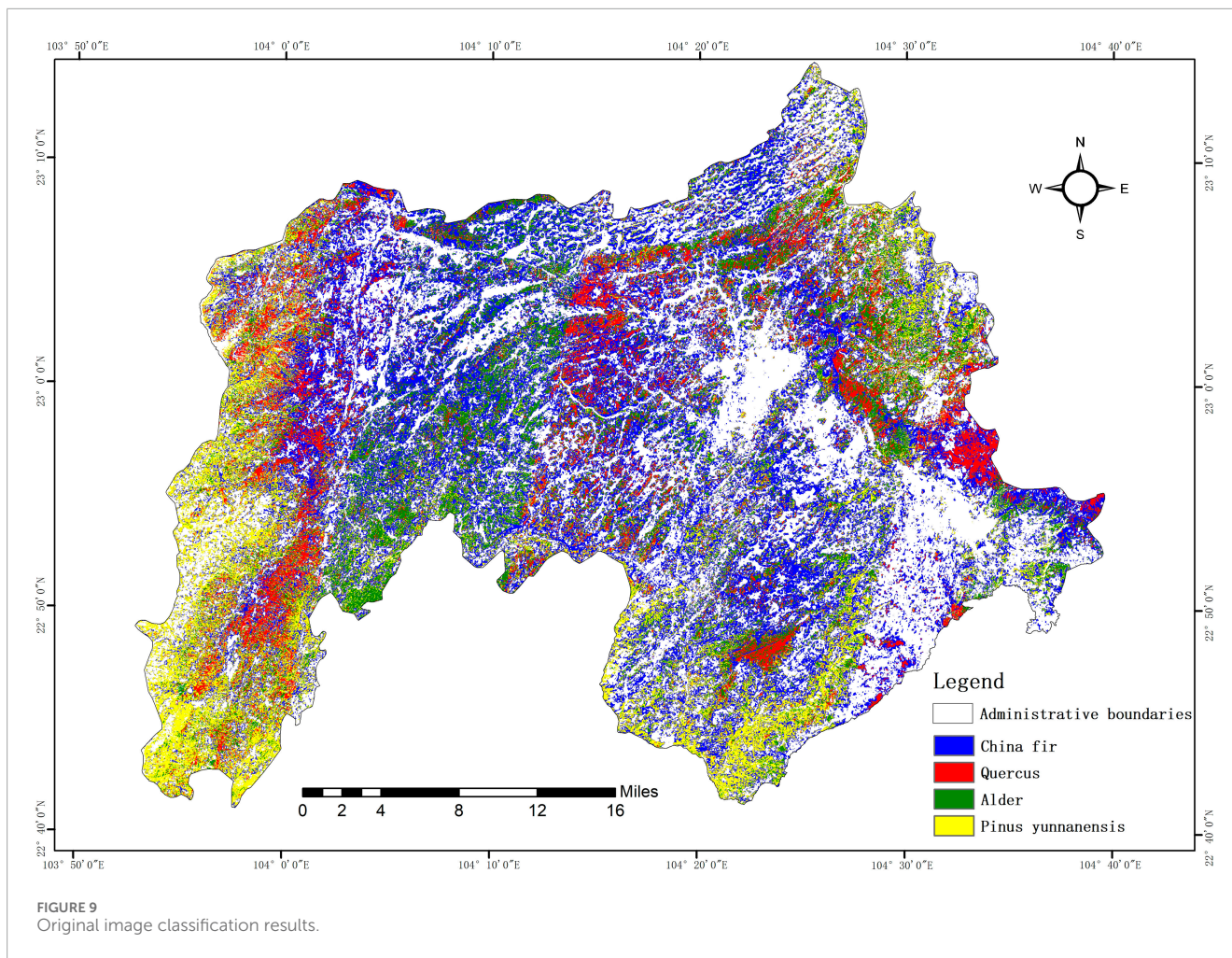
where  $n$  is the number of spectral bands,  $x_i$  and  $y_i$  represent the response values of the two spectral vectors in the  $i$ -th band, and  $\alpha$  is the spectral angle whose range of variation is  $[0, \pi/2]$ . The values of the pixels in the spectral angle image can also be expressed using  $\cos(\alpha)$ , which has a variation range of  $[0, 1]$ .

### 3.4 Accuracy verification

The Confusion Matrix, also known as the Error Matrix, can accurately reflect the classification results and ground truth information, and reflect the final classification accuracy in a

TABLE 3 Spectral bands with significant differences.

Spectral category	Significant difference band/nm
Original spectrum	395–516, 662–682, 774–794, 825–845, 851–872, 937–957, 1,055–1,075, 1,139–1,159, 1,173–1,193, 1,245–1,265, 1,459–1,479, 1,644–1,664, 1,650–1,670, 2,199–2,219
First-order differential spectrum	500–520, 516–536, 559–579, 557–577, 712–732, 995–1,115, 1,129–1,149, 1,482–1,502, 1701–1721, 2021–2041
Second-order differential spectrum	547–567, 670–690, 687–707, 1,129–1,149, 1,146–1,166
De-enveloped spectrum	480–500, 532–552, 1,180–1,200, 1,667–1,687



Confusion Matrix. Each column of the confusion matrix represents a ground truth classification, and the value in each column is equal to the number of ground truth pixels corresponding to the corresponding category in the classification image. There are two types of pixel count and percentage representation. By calculating the confusion matrix, two indicators, Overall Accuracy and Kappa coefficient, can be obtained, and the research results can be validated by combining them.

The overall classification accuracy is equal to the correctly classified pixels Eq. (5). The number of correctly classified pixels is distributed along the diagonal of the confusion matrix, and the total number of pixels is equal to the total number of pixels of all real reference sources. The overall classification accuracy calculation formula (5) is shown.

$$OA = \frac{pixel_{true}}{pixel_{all}} \tag{5}$$

In Eq. 5, it represents the overall classification accuracy, is the correct number of pixels for classification, is the total number of pixels.

Kappa coefficient: It is the sum of the total number of real reference pixels  $N$ ) multiplied by the diagonal of the confusion matrix  $(X_{kk})$ , subtracted by the product of the number of real reference pixels in a certain class and the total number of classified

pixels in that class, and then divided by the square of the total number of pixels and subtracted by the product of the total number of real reference pixels in a certain class and the total number of classified pixels in that class to sum all categories Eq. (6). The calculation formula is as follows.

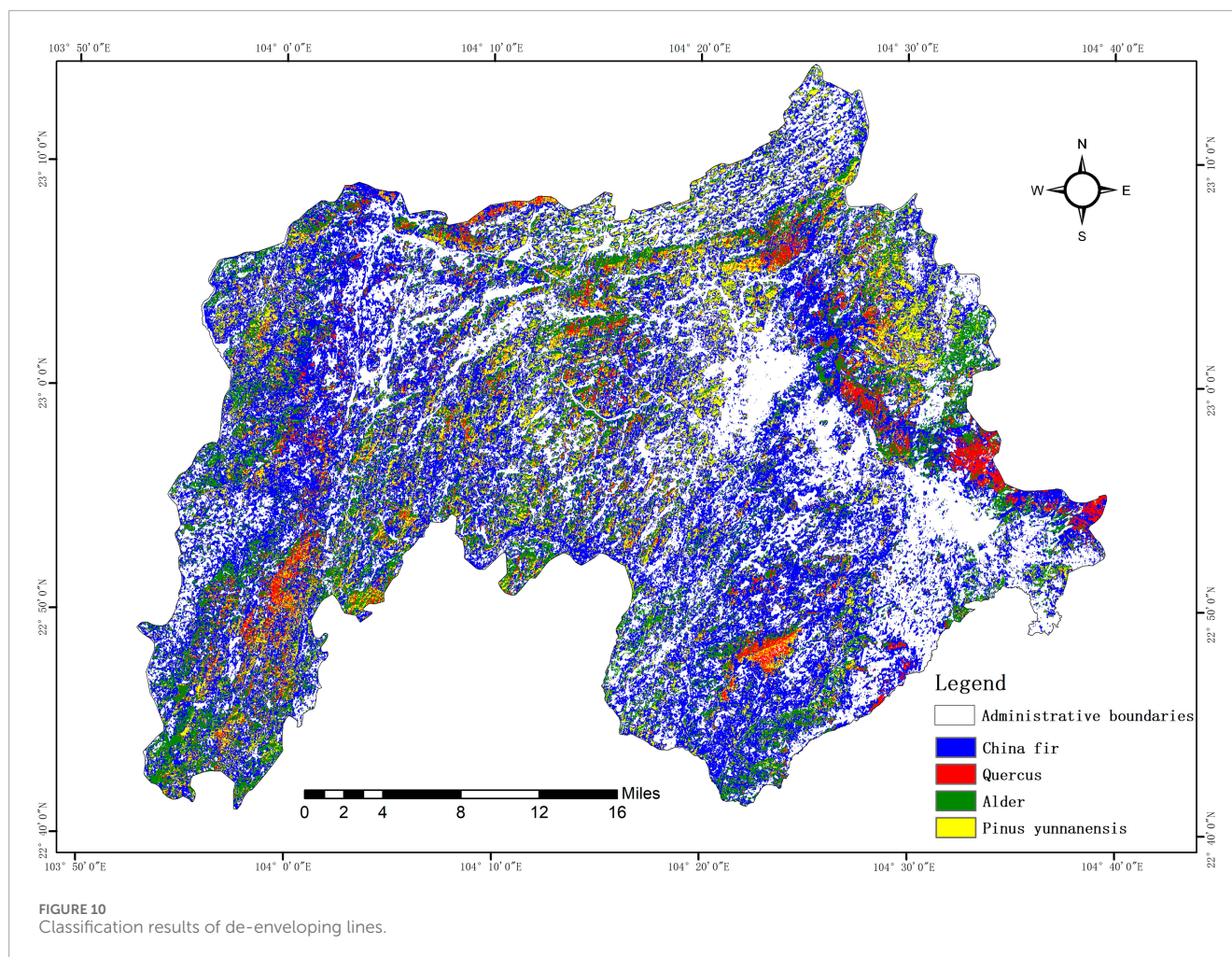
$$K = \frac{N \sum_k^X - \sum_k^X k \sum_k^X k}{N^2 - \sum_k^X k \sum_k^X k} \tag{6}$$

## 4 Analysis of spectral characteristic curve transformation results

### 4.1 Original spectral characteristic curve

The original spectral characteristic curves for the four tree species in the study area (Quercus, Alder, China fir, and *P. yunnanensis*) obtained after sampling from the preprocessed Resource-1 02D hyperspectral image data are shown in Figure 5.

Figure 5 indicates that all four tree species exhibited typical vegetation spectral characteristics, with spectral reflectance increasing then decreasing with the wavelength. Within the



wavelength range of 395–996nm, the spectral curves of China fir and Alder overlapped in the range of 775–988 nm. All four tree species showed a reflection peak around 550 nm, with reflectance decreasing between 550 and 679 nm. In this range, distinguishing between China fir and Alder was difficult because their spectral curves overlapped. In the range of 775–988 nm, spectral reflectance of the four tree species was in the order of  $P. yunnanensis > Quercus > Alder > China\ fir$ , indicating distinct differences in reflectance among the four. These differences are favorable for classification. In the range of 1,005–1,173 nm, the spectral reflectance of the four tree species differed considerably, and at 1,072 nm, reflectance reached its maximum value, which was also beneficial for species classification. Within the ranges of 1,459–1,778 and 1,997–2,450 nm, substantial differences in spectral reflectance were observed among the four tree species, which also facilitated tree species classification.

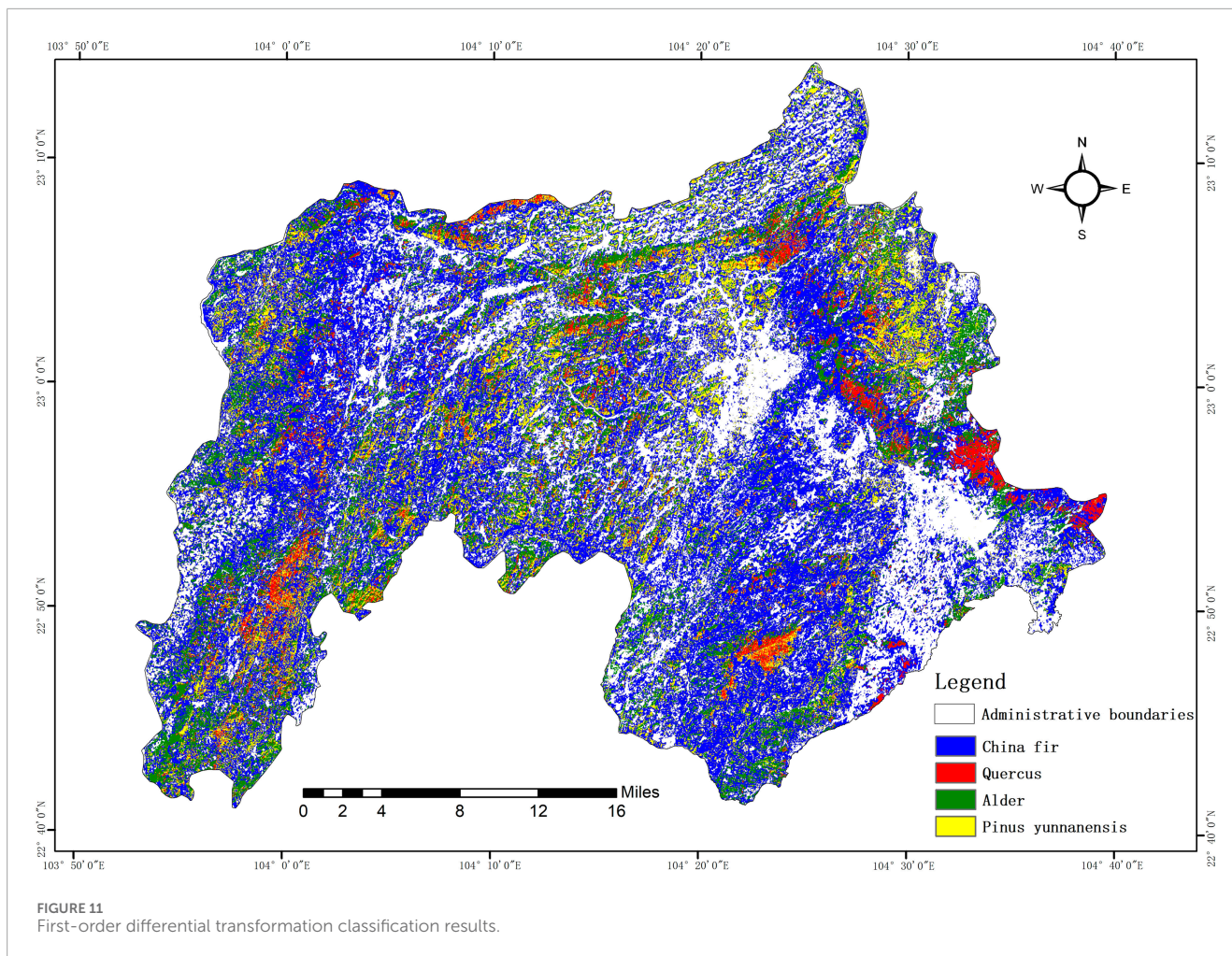
## 4.2 Spectral characteristic curves after first-order differential transformation

The spectral curve characteristics of vegetation are amplified after first-order differential transformation. The spectral

characteristic curves of *Quercus*, Alder, China fir, and *P. yunnanensis* are shown in Figure 6.

Figure 6 indicates that the spectral characteristic curves of the four tree species exhibited considerable differences. Within the range of 395–413 nm, the curves showed a decreasing trend, but the first-order differential curves of *Quercus* and *P. yunnanensis* overlapped and could not be distinguished. In the range of 413–499 nm, the spectral characteristic curves of the four tree species completely overlapped, making them indistinguishable. Within the range of 499–550 nm, the first-order differentials for the four tree species were positive, indicating a positive correlation between their spectral reflectance and wavelength. Additionally, all four tree species exhibited a reflectance peak at 524 nm. Within the range of 559–679 nm, the first-order differential values were negative, and the frequency and amplitude were similar, suggesting a negative correlation between spectral reflectance and wavelength. However, the first-order differential values were ineffective in distinguishing tree species in this range because of their high overlap degree. Within the range of 687–765 nm, the first-order differential values of the four tree species were in the order of  $P. yunnanensis > Quercus > China\ fir > Alder$ . At 730 nm, all four tree species exhibited a maximum first-order differential reflectance peak, and the differences were substantial. Therefore, 730 nm can





serve as a feature band for classifying tree species. Another sensitive range was the reflectance peak from 1,475 to 1,644 nm, with the peak located at 1,526 nm. Within this range, the first-order differential values of the four tree species were in the order of *P. yunnanensis* > *Quercus* > *China fir* > *Alder*, making this range a sensitive band that can be used for differentiation. Moreover, a sensitive band region was found in the range of 1,660–1,750 nm, where a negative peak appeared. The spectral first-order differential values of the four tree species in this range were in the order of *Alder* > *China fir* > *Quercus* > *P. yunnanensis*. A negative peak was observed at 1,711 nm, which can be used as a distinguishing feature band.

### 4.3 Spectral characteristic curves after second-order differential transformation

The spectral characteristic curves of *Quercus*, *Alder*, *China fir*, and *P. yunnanensis* after second-order differential transformation are shown in [Figure 7](#).

[Figure 7](#) reveals considerable differences in the regions between 524–567 and 622–722 nm. In the range of 524–567 nm, a second-order differential negative peak centered at 550 nm was found, with the second-order differential spectral values ranking in the order

of *China fir* > *Alder* > *P. yunnanensis* > *Quercus*. In the range of 622–722 nm, a second-order differential reflectance peak centered at 696 nm was observed, with the second-order differential spectral values ranking in the order of *Quercus* > *P. yunnanensis* > *Alder* > *China fir*. The two ranges were effective in distinguishing the four tree species. In the ranges of 928–954 and 1,105–1,173 nm, substantial fluctuation was observed in the second-order differential values of the four bands, which can serve as feature bands for distinguishing the four tree species. Within the 928–954 nm range, the second-order differential value of *Quercus* was considerably different from the values of the three other species. *Alder*, *China fir*, and *P. yunnanensis* had similar second-order differential values. In the 1,105–1,173 nm range, the reflectance of *Quercus* peaked at 1,139 nm, and the reflectance of *Alder*, *China fir*, and *P. yunnanensis* peaked at 1,156 nm.

### 4.4 Spectral characteristic curve after envelope removal

The spectral characteristic curves of *Quercus*, *Alder*, *China fir*, and *P. yunnanensis* after envelope removal are shown in [Figure 8](#).

[Figure 8](#) shows considerable differences in the spectral characteristic curves of the four tree species. At 500 nm, a

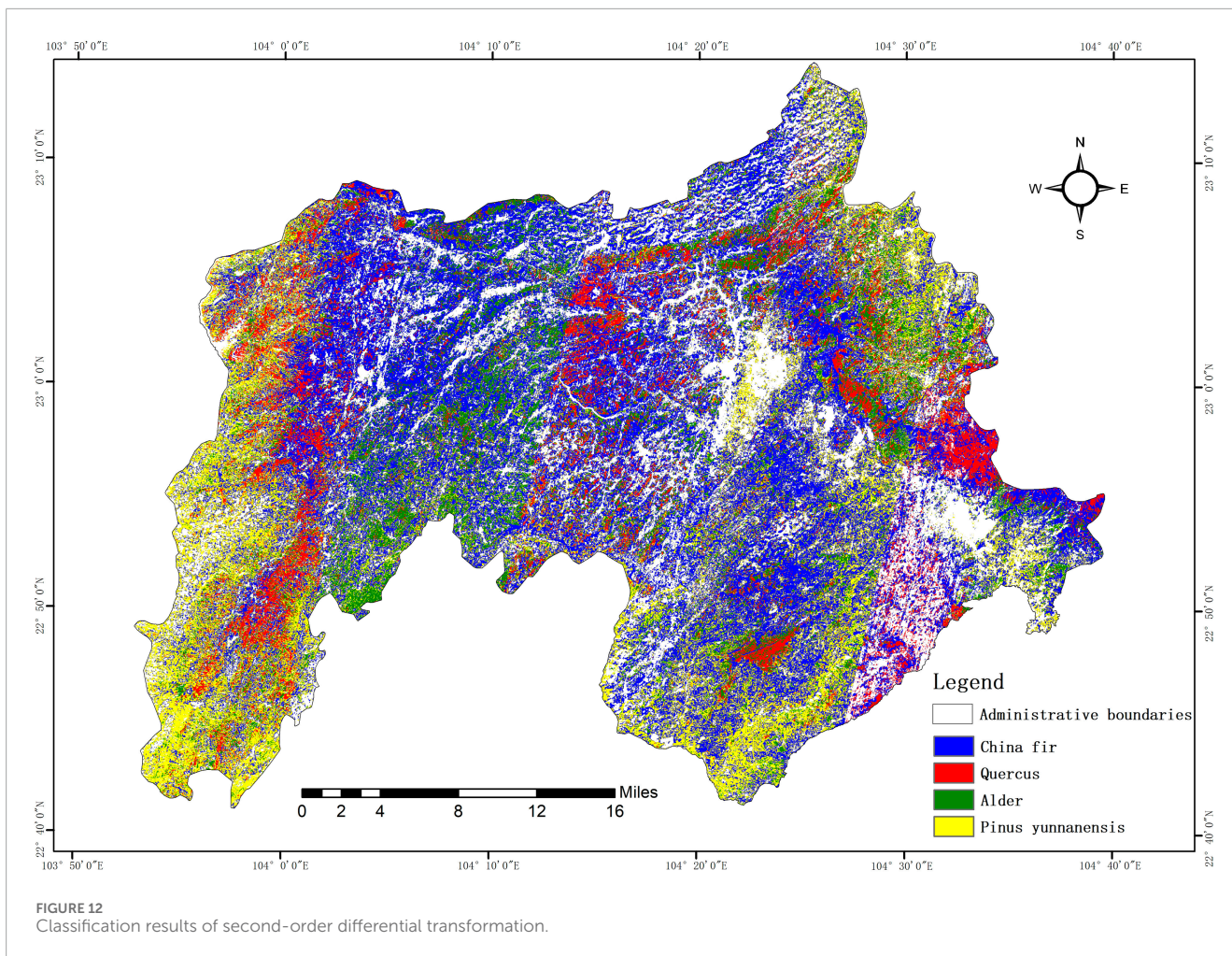


**TABLE 4** Overall accuracy and kappa coefficient statistics.

Category	Overall accuracy/%	Kappa coefficient
Original image spectrum	88.71	0.85
Envelope removal method	95.59	0.94
First-order differential spectrum	97.18	0.96
Second-order differential spectrum	81.69	0.76

pronounced absorption valley was found, and reflectance was in the order of Quercus > Alder > China fir > P. yunnanensis. At 550 nm, a clear absorption peak was observed, and reflectance was in the order of Quercus > China fir > Alder > P. yunnanensis. At 1,660 nm, a distinct absorption peak was found, and reflectance was in the order of Quercus > Alder > P. yunnanensis > China fir. The three wavelengths were effective for distinguishing the four tree species.

In conclusion, after analyzing the curve feature differences in the preprocessed original spectrum, first-order differential spectrum,

second-order differential spectrum, and the spectrum after envelope removal, wavelengths were selected in units of 20 nm from the four types of spectral curves, resulting in 14, 10, 5, and 4 wavelengths, as shown in Table 3. The selected wavelengths were then used for tree species classification.

## 5 Classification results and accuracy evaluation

### 5.1 Classification results

The pixel spectral curves of the four tree species were analyzed through a field investigation of 226 forest stands. The average spectral curves were used as the spectral reference curves for each tree species. The spectral angle mapping method was employed to classify tree species in the Resource Satellite 02D imagery. The classification results are shown in Figures 9–12. Figure 9 presents the classification results of the preprocessed original image, Figure 11 displays the classification results after envelope removal, Figure 11 shows the classification results after first-order differential transformation, and Figure 12 illustrates the classification results after second-order differential transformation.

The analysis and comparison of the results revealed that the classification results for the images processed with envelope removal and first-order differential transformation were highly accurate. The classification results for the preprocessed original image and the images processed with second-order differential transformation had low accuracy. The areas with misclassification were mainly the planting areas of *P. yunnanensis* and China fir. Some China fir areas were misclassified as *P. yunnanensis* areas, and a small portion of China fir was misclassified as *Quercus*.

## 5.2 Precision evaluation

In this study, the accuracy of the classification results was validated using a confusion matrix method (Gonzalez-Alonso et al., 1997). Based on the distribution of tree species in the study area, a total of 226 sampling points were set up, including 68 samples of China fir, 51 samples of Oak, 68 samples of Alder, and 39 samples of *Pinus yunnanensis*. A total of 288 pixels were obtained from the validation sample points, including 69 for *Pinus yunnanensis*, 80 for Alder, 75 for Oak, and 64 for China fir. Overall accuracy and the kappa coefficient were used to assess accuracy. Seventy-five percent of the sample pixels were used for classification, and the remaining 25% was used for accuracy validation. The results, which are shown in Table 4, indicate that the classification result from the image processed with second-order differential transformation had the lowest overall accuracy (81.69%) among all the classification results primarily because of the misclassification among *P. yunnanensis*, China fir, and *Quercus*. The classification result from the original image (overall accuracy of 88.71%) was slightly higher than that from second-order differential transformation. The accuracy of the classification results for the images processed with envelope removal and first-order differential transformation exceeded 95%, and these results closely matched the field survey data.

## 6 Conclusion and discussion

### 6.1 Conclusion

This study adopted forestry field survey data for Maguan County in Yunnan and Resource Sat-2 hyperspectral satellite imagery. It also employed three methods, namely, first-order differentiation, second-order differentiation, and envelope removal, to analyze the spectral characteristics of four dominant tree species in Maguan County. The SAM technique was applied for tree species classification, and accuracy validation was conducted. According to the experimental results, the imagery data processed with first-order differentiation and envelope removal effectively enhanced the differentiation between bands and improved the accuracy of species classification. The original imagery and the imagery processed with second-order differentiation had low classification accuracy and showed instances of misclassification. The threshold setting of the matching angle might have affected the spectral classification or complexities in the land cover distribution within mixed pixels and made it challenging to describe real-world objects accurately, resulting in the aforementioned misclassification.

Moreover, during the data preprocessing phase, the imagery subjected to atmospheric correction showed that although the spectral characteristics of the vegetation were corrected, the reflectance values were low, which can lead to “same material, different spectrum” or “same spectrum, different material” issues (Zhang et al., 2006; Huang et al., 2022). These factors can also affect classification accuracy.

In summary, using hyperspectral remote sensing data in tree species classification is highly feasible. Methods, such as first-order differentiation and envelope removal, effectively enhance the spectral characteristics of vegetation. Additionally, the use of SAM for classification considerably improves the accuracy of tree species classification.

### 6.2 Discussion

Currently, hyperspectral data are a reliable data source for tree species classification and can be applied to fine-scale tree species classification in the field of remote sensing. However, previous studies encountered challenges in balancing data processing speed, quality, and accuracy. This research combined three methods, namely, first-order differentiation, second-order differentiation, and envelope removal, with SAM to achieve satisfactory classification results for the study area. However, the study still has some limitations. For instance, the selection of certain tree species areas as the basis for generating average spectral feature curves may lead to inaccuracies if other land cover types exist within the selected regions. Future research should choose pure pixel samples as much as possible and collect ground-truth spectral data through field surveys to further validate the spectral feature curves, thus reducing the influence of other land cover types on the final results. Furthermore, this study focused on Maguan County. Future research could apply the geographic third law to classify and validate tree species with similar geographical environments (Zhu et al., 2018).

### Data availability statement

The original contributions presented in the study are included in the article/supplementary material, further inquiries can be directed to the corresponding author.

### Author contributions

JZ: Writing–review and editing, Writing–original draft, Visualization, Validation, Supervision, Resources, Methodology, Investigation, Funding acquisition, Formal Analysis, Conceptualization. ZF: Writing–review and editing, Writing–original draft, Visualization, Validation, Project administration, Methodology, Formal Analysis, Data curation, Conceptualization. YL: Writing–review and editing, Visualization, Project administration, Methodology, Investigation, Conceptualization. WJ: Writing–review and editing, Visualization, Validation, Funding acquisition, Supervision, Methodology. XM: Writing–review and editing, Validation, Supervision, Methodology,

Formal Analysis. YL: Writing–review and editing, Visualization, Validation, Supervision, Software. SQ: Writing–review and editing, Visualization, Validation, Supervision, Methodology.

## Funding

The author(s) declare that financial support was received for the research, authorship, and/or publication of this article. This research was funded by the Funding for Yunnan Province Graduate Supervisor Team Construction Project. Science and Technology Major Project of Yunnan Province (Science and Technology Special Project of Southwest United Graduate School–Major Projects of Basic Research and Applied Basic Research): Vegetation change monitoring and ecological restoration models in Jinsha River Basin mining area in Yunnan based on multi-modal remote sensing (Grant No. : 202302AO370003). The Multi-government International Science and Technology Innovation Cooperation Key Project of the National Key Research and Development Program of China for the “Environmental monitoring and assessment of land use/land cover change impact on ecological security using geospatial technologies”(2018YFE0184300).

## References

- Boyd, D. S., and Danson, F. (2005). Satellite remote sensing of forest resources: three decades of research development. *Prog. Phys. Geogr.* 29 (1), 1–26. doi:10.1191/0309133305pp432ra
- Ding, L., Wang, Z., and Ge, H. (2010). Continuum removal based hyperspectral characteristic analysis of leaves of different tree species. *J. Zhejiang A F Univ.* 27 (06), 809–814. doi:10.11833/j.issn.2095-0756.2010.06.001
- Evans, G. (1939). Ecological studies on the rain forest of southern Nigeria: II. The Atmospheric Environmental Conditions. *J. Ecol.* 27, 436–482. doi:10.2307/2256374
- Gong, P., Pu, R., and Yu, B. (1997). Conifer species recognition: an exploratory analysis of *in situ* hyperspectral data. *Remote Sens. Environ.* 62 (2), 189–200. doi:10.1016/s0034-4257(97)00094-1
- Gong, P., Pu, R., and Yu, B. (1998). Conifer species recognition with seasonal hyperspectral data. *Natl. Remote Sens. Bull.* (03), 211–217.
- Gonzalez-Alonso, E., Cuevas, J. M., and Arbiol, R. (1997). Remote sensing and agricultural statistics: crop area estimation in north-eastern Spain through diachronic Landsat TM and ground sample data. *Int. J. Remote Sens.* 18 (2), 467–470. doi:10.1080/014311697219213
- Goodenough, D. G., Bhogal, A., Dyk, A., Hollinger, A., Mah, Z., Niemann, K. O., et al. (2002). “Monitoring forests with hyperion and ALI” in IEEE International Geoscience and Remote Sensing Symposium, Toronto, ON, Canada, November 07, 2002 (IEEE).
- Gu, X., Wang, Y., Sun, Q., Yang, G., and Zhang, C. (2019). Hyperspectral inversion of soil organic matter content in cultivated land based on wavelet transform. *Comput. Electron. Agric.* 167, 105053. doi:10.1016/j.compag.2019.105053
- Herawati, H., and Santoso, H. (2011). Tropical forest susceptibility to and risk of fire under changing climate: a review of fire nature, policy and institutions in Indonesia. *For. Policy Econ.* 13 (4), 227–233. doi:10.1016/j.forpol.2011.02.006
- Huang, P., Pu, J., Zhao, Q., Li, Z., Song, H., and Zhao, X. (2022). Research progress and development trend of remote sensing information extraction methods of vegetation. *Remote Sens. Nat. Resour.* 34 (2), 10–19. doi:10.6046/zrzyyg.2021137
- Kokaly, R. F., and Clark, R. N. (1999). Spectroscopic determination of leaf biochemistry using band-depth analysis of absorption features and stepwise multiple linear regression. *Remote Sens. Environ.* 67 (3), 267–287. doi:10.1016/S0034-4257(98)00084-4
- Kruse, F. A., Lefkoff, A., Boardman, J., Heidebrecht, K., Shapiro, A., Barloon, P., et al. (1993). The spectral image processing system (SIPS)—interactive visualization and analysis of imaging spectrometer data. *Remote Sens. Environ.* 44 (2–3), 145–163. doi:10.1016/0034-4257(93)90013-n
- Kumar, L., Skidmore, A. K., and Mutanga, O. (2010). Leaf level experiments to discriminate between eucalyptus species using high spectral resolution reflectance data: use of derivatives, ratios and vegetation indices. *Geocarto Int.* 25 (4), 327–344. doi:10.1080/10106040903505996
- Leckie, D. G. (1990). Advances in remote sensing technologies for forest surveys and management. *Can. J. For. Res.* 20 (4), 464–483. doi:10.1139/x90-063
- Lei, G., Li, A., Tan, J., Zhang, Z., Bian, J., Jin, H., et al. (2016). Forest types mapping in mountainous area using multi-source and multi-temporal satellite images and decision tree models. *Remote Sens. Technol. Appl.* 31 (01), 31–41. doi:10.11873/i.issn.1004-0323.2016.1.0031
- Liu, J., Gao, G., Wang, S., Jiao, L., Wu, X., and Fu, B. (2018). The effects of vegetation on runoff and soil loss: multidimensional structure analysis and scale characteristics. *J. Geogr. Sci.* 28, 59–78. doi:10.1007/s11442-018-1459-z
- Liu, Y. (2021). *Study on hyperspectral identification Model of typical treeSpecies in changting county.* doi:10.27019/d.cnki.gfjsu.2021.000320
- Ma, C., Liu, X., Li, S., Li, C., and Zhang, R. (2023). Accuracy evaluation of hyperspectral inversion of environmental parameters of loess profile. *Environ. Earth Sci.* 82 (10), 251. doi:10.1007/s12665-023-10873-8
- Martin, M., Newman, S. D., Aber, J. D., and Congalton, R. G. (1998). Determining forest species composition using high spectral resolution remote sensing data. *Remote Sens. Environ.* 65 (3), 249–254. doi:10.1016/S0034-4257(98)00035-2
- Meng, X., Bao, Y., Liu, H., Zhang, A., Liu, Y., and Wang, D. (2020). Soil classification of typical black soil areas in Northeast China based on high-resolution image No.5. *Trans. Chin. Soc. Agric. Eng.* 36 (16). doi:10.11975/j.issn.1002-6819.2020.16.028
- Molchanov, A. A. (1963). *The hydrological role of forests.*
- Pasquarella, V. J., Holden, C. E., and Woodcock, C. E. (2018). Improved mapping of forest type using spectral-temporal Landsat features. *Remote Sens. Environ.* 210, 193–207. doi:10.1016/j.rse.2018.02.064
- Petropoulos, G. P., Vadrevu, K. P., and Kalaitzidis, C. (2013). Spectral angle mapper and object-based classification combined with hyperspectral remote sensing imagery for obtaining land use/cover mapping in a Mediterranean region. *Geocarto Int.* 28 (2), 114–129. doi:10.1080/10106049.2012.668950
- Ren, Z., Sun, L., and Zhai, Q. (2020). Improved k-means and spectral matching for hyperspectral mineral mapping. *Int. J. Appl. Earth Observation Geoinformation* 91, 102154. doi:10.1016/j.jag.2020.102154
- Rong, Y., Yan, Y., Zhao, C., Wang, C., Shang, X., Zhu, J., et al. (2022). Straw checkboard or afforestation? Assessment and comparison of combined benefits of

## Acknowledgments

We appreciate the forestry data provided by the Forestry Bureau of Maguan County; Free 30 m resolution DEM data and Landsat provided by Geospatial Data Cloud8OLI data; The land observation satellite data service platform provides hyperspectral remote sensing image data.

## Conflict of interest

The authors declare that the research was conducted in the absence of any commercial or financial relationships that could be construed as a potential conflict of interest.

## Publisher’s note

All claims expressed in this article are solely those of the authors and do not necessarily represent those of their affiliated organizations, or those of the publisher, the editors and the reviewers. Any product that may be evaluated in this article, or claim that may be made by its manufacturer, is not guaranteed or endorsed by the publisher.

- two typical sand fixing models. *J. Clean. Prod.* 358, 131924. doi:10.1016/j.jclepro.2022.131924
- Roush, T., and Clark, R. (1984). *Reflectance spectroscopy-quantitative analysis techniques for remote sensing applications*. Journal of Geophysical Research. Washington, D.C., United States. American Geophysical Union. 87, 6329–40. doi:10.1029/jb089ib07p06329
- Sayer, J., Chokkalingam, U., and Poulsen, J. (2004). The restoration of forest biodiversity and ecological values. *For. Ecol. Manag.* 201 (1), 3–11. doi:10.1016/j.foreco.2004.06.008
- Shen, C. (2022). *Dongchuan red soil Based on GF-5 spectral feature analysis Research on surface cover identification*. Master. Kunming, China: Kunming University of Science and Technology. doi:10.27200/d.cnki.gkmlu.2022.000960
- Shu, T., Yue, Y., Li, L., Li, R., Li, Y., and Peng, Z. (2016). Crop identification based on hyperspectral remote sensing. *Jiangsu J. Agric. Sci.* 32 (06), 1310–1314. doi:10.3969/j.issn.1000-4440.2016.06.018
- Sovacool, B. K. (2014). Environmental issues, climate changes, and energy security in developing Asia. *SSRN Electron. J.* doi:10.2139/ssrn.2479725
- Sun, H., Liu, N., Xing, Z., Zhang, Z., Li, M., and Wu, J. (2019). Parameter Optimization of potato spectral response characteristics and growth stage Identification. *Spectrosc. Spectr. Analysis* 39 (06), 1870–1877. doi:10.3964/j.issn.1000-0593(2019)06-1870-08
- Thompson, I., Mackey, B., McNulty, S., and Mosseler, A. (2009). *Forest resilience, biodiversity, and climate change. A synthesis of the biodiversity/resilience/stability relationship in forest ecosystems*. Montreal, Canada: Secretariat of the Convention on Biological Diversity
- Wang, L., and Fan, W. (2015). Hyperspectral remote sensing data for identifying dominant forest tree species group. *J. Northeast For. Univ.* 43 (05), 134–137. doi:10.13759/j.cnki.dlxb.20150522.030
- Wang, Z. (2011). *Application Of Hyperspectral Remote Sensing In Forest Tree Species Discrimination*. Master. Hangzhou, China: Zhejiang A&F University.
- Xie, B., Xue, X., Liu, W., Wang, J., and Wang, G. (2005). Hull-curve-method-based extraction and analysis of soilspectral characteristics. *Acta Pedol. Sin.* (01), 171–175. doi:10.3321/j.issn:0564-3929.2005.01.029
- Xu, Z., Xu, J., Yu, K., Gong, C., Xie, W., Lai, R., et al. (2013). Spectral features analysis of *Pinus massoniana* with pest of *dendrolimus punctatus* walker and levels detection. *Spectrosc. Spectr. Analysis* 33 (02), 428–433. doi:10.3964/j.issn.1000-0593(2013)02-0428-06
- Yang, C., Feng, M., Song, L., Wang, C., Yang, W., Xie, Y., et al. (2021). Study on hyperspectral estimation model of soil organic carbon content in the wheat field under different water treatments. *Sci. Rep.* 11 (1), 18582. doi:10.1038/s41598-021-98143-0
- Yu, L. (2013). *The Explore of forest tree species discrimination Based on hyperspectral remote sensing data*. Master. Fuzhou, China: Fujian Normal University.
- Yu, L., Yu, Y., Liu, X., Du, Y., and Zhang, H. (2016). Tree species classification with hyperspectral Image. *J. Northeast For. Univ.* 44 (09), 40–43+57. doi:10.13759/j.cnki.dlxb.2016.09.009
- Zhang, C., Mu, Y., Yan, T., and Chen, Z. (2018). Overview of hyperspectral remote sensing technology. *Spacecr. Recovery and Remote Sens.* 39 (3), 104–114. doi:10.3969/j.issn.1009-8518.2018.03.012
- Zhang, H., Jiang, J., Xie, X., Wu, H., and Zhang, L. (2006). Classification of TM imagery based on the Improved BP neural network algorithm. *J. Agric. Mech. Res.* (10), 55–57. doi:10.13427/j.cnki.njyi.2006.10.018
- Zhang, X., and Li, P. (2014). Lithological mapping from hyperspectral data by improved use of spectral angle mapper. *Int. J. Appl. Earth Observation Geoinformation* 31, 95–109. doi:10.1016/j.jag.2014.03.007
- Zhong, H., Liu, H., and Lin, W. (2021). Application of lidar and hyperspectral remote sensing technology to tree species identification. *World For. Res.* 34 (04), 41–45. doi:10.13348/j.cnki.sjlyyj.2021.0013.y
- Zhu, A. X., Lu, G., Liu, J., Qin, C. Z., and Zhou, C. (2018). Spatial prediction based on third law of geography. *Ann. GIS* 24 (4), 225–240. doi:10.1080/19475683.2018.1534890